Superlattices and Microstructures 159 (2021) 107034

Contents lists available at ScienceDirect

Superlattices and Microstructures

journal homepage: www.elsevier.com/locate/superlattices

Comparison of characteristic properties of Al, Ga, and In-doped ZnO thin films formed by sol-gel method

Seyda Horzum [a,*], Emel Bulduk [b], Deniz Şener [b], Tülay Serin [b]

[a] Integrated Research Centers, Izmir Institute of Technology, 35430, Izmir, Turkey
[b] Department of Physics Engineering, Ankara University, 06100, Tandoğan, Ankara, Turkey

ARTICLE INFO

Keywords:
Thin films
Sol-gel deposition
ZnO
Raman spectroscopy

ABSTRACT

Herein, we examine the effect of doping with Indium (In), Gallium (Ga), and Aluminum (Al) (group III elements) on the structural, optical, and vibrational properties of ZnO thin films. The characteristic properties of the ZnO films prepared by the sol-gel dip-coating method are explored by utilizing X-ray diffraction, optical spectroscopy, and Raman scattering measurements. XRD analyzes exhibit that the crystallite size reduces upon doping by Ga and Al, while it increases with In, and all films have hexagonal wurtzite structure. Additionally, Raman measurements indicate that the dominant two peaks at around 104 and 445 cm^{-1} are related to E_2^{low} and E_2^{high} phonon modes of ZnO, respectively. The low-frequency mode (E_2^{low}) is affected by dopant atoms, whereas the high-frequency mode (E_2^{high}) of the wurtzite phase is not influenced by the dopant. Moreover, $E_{dop\text{-}atom}$ phonon mode appears at low frequencies and the intensity ratio, $I(E_{dop.atom})/I(E_2^{low})$, decreases as the ionic radius of dopant atoms increases. UV–Vis spectra reveal that the film transparency, optical band gap, Urbach energy, and refraction index can be effectively tuned by dopant atoms.

1. Introduction

Zinc oxide (ZnO) is one of the mostly studied metal oxides with its remarkable optical and electrical properties [1,2]. It is widely used in diverse applications, such as lasers, detectors, LEDs, thin-film transistors, and solar cells with its wide band gap [3–13]. To develop and control the characteristic properties of ZnO films, doping with different atoms is an efficient method. So far, the doping of ZnO with several atoms such as Li, Ag, Cu, Ga, etc. has been extensively studied by many researchers. Nayak et al. showed that sufficient Li doping causes a significant reduction in the conductivity of ZnO films and also improves the orientation of ZnO crystallites along the c-axis [14]. Ahn et al. examined the effect of Ag content in ZnO by means of thermal analysis and showed that Ag-doped ZnO has p-type conduction by the electrical and structural analysis [15]. Horzum et al. demonstrated that the Cu-doped ZnO thin films have electronic defect states originating from copper atoms [16]. They also stated that Cu-doped ZnO films are passive as optically and the band edges of ZnO compose the optical band gap. In another study, Horzum et al. also investigated that how vibrational and structural properties of zinc oxide changed with gallium doping [17]. They observed the additional phonon mode (E_{Ga}) originating from gallium atoms at low-frequency values in the Raman spectrum of Ga-doped ZnO. It is also demonstrated that the intensity ratio of the peaks of E_{Ga} and E_2^{low} which are located at low frequency depends on the amount of doping in the ZnO. Russo et al. reported the relationship

* Corresponding author.
E-mail addresses: seydahorzum@iyte.edu.tr (S. Horzum), emelbldk@gmail.com (E. Bulduk), dnzsener@gmail.com (D. Şener), serin@eng.ankara.edu.tr (T. Serin).

https://doi.org/10.1016/j.spmi.2021.107034
Received 18 May 2021; Received in revised form 14 August 2021; Accepted 13 September 2021
Available online 14 September 2021

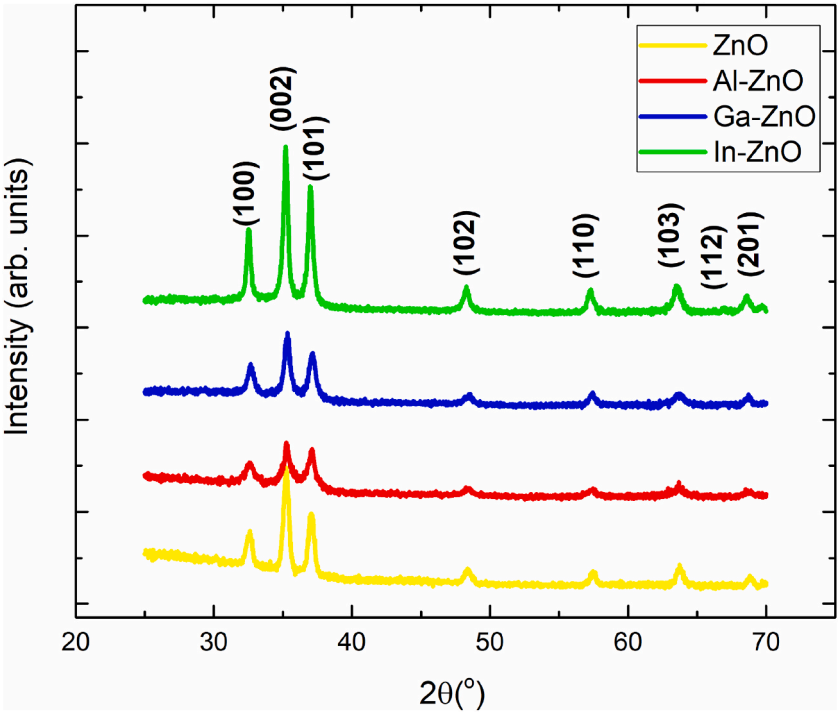

Fig. 1. XRD patterns of undoped and doped ZnO thin films.

between Raman spectra and electronic properties of Al-doped ZnO films [18]. The variation on structural, optical, and morphological properties of ZnO with indium doping is examined by Tyona et al. [19]. They performed that indium doping improves the photovoltaic performance of ZnO electrodes. Among these dopants, group III elements such as Al, Ga, or In have been attracted due to the increase in the functionality of ZnO in device applications [20]. It is well known that the ionic radius of Ga^{3+} (0.62 Å) and Al^{3+} (0.53 Å) are lower than that of Zn^{+2} (0.74 Å), while the ionic radius of In (0.80 Å) is greater than that of Zn^{2+}. Although many studies focus on doping of ZnO by various atoms, the study comparing the effects of dopant atoms on especially vibrational properties is quite rare. This study aims to compare the effects of Al, Ga, and In dopants on the characteristic properties of ZnO thin films obtained by the sol-gel dip--coating method. The vibrational, optical, and structural properties of doped ZnO thin films are analysed by Raman, UV–Vis–NIR, and XRD measurements, respectively.

2. Experimental

Al, In, Ga doped and undoped ZnO thin films are deposited on glass substrates by the sol-gel dip-coating method. First, Zinc acetate-2-hydrate [$Zn(CH_3COO)_2{\cdot}2H_2O$] which is starting material is dissolved in ethyl alcohol (C_2H_5OH). Then, Diethanolamine [$HN(CH_2CH_2OH]_2$ is added to the solution as a stabilizer in a molar ratio DEA/Zn = 1. $InCl_3$, $AlCl_3$, and Ga $(NO_3)_xH_2O$ are used as In, Al, and Ga sources. The amount of dopant in the solution is adjusted to be 3 wt %. Before the coating process, the solution is aged 24 h at room temperature. After each dipping period, the films are heated at 500 °C for 10 min in the air atmosphere. This process is repeated 10 times to increase the film thickness. The structural characterization of ZnO films is performed by recording X-ray diffraction data in the 2θ scanning range of 25–70° using Rigaku Miniflex 600 Table Top Powder X-ray diffractometer CuK_α radiation source with a wavelength of 0.154 nm. Raman measurements are carried out using Horiba XploRA Raman spectrometer. Raman-scattered light is collected using Olympus Bx41 transmission and reflection illumination microscope (Olympus, France) with a 100 × objective magnification (NA = 0.90). To enroll the Raman signals, the green laser excitation of 532 nm is used by grating 1200 grooves/mm in a spectral range of 50–800 cm^{-1}. Optical measurements are implemented by UV–VIS–NIR Shimadzu 3600 spectrophotometer in the spectral region 300–1600 nm.

3. Results and discussion

3.1. Structural properties

To identify the impact of doping on the structural properties of ZnO, the XRD spectra are investigated. As seen in Fig. 1, the films have main peaks in (100), (002), (101), and weak peaks in (102), (110), (103), (112), and (201). The obtained peaks agree with the hexagonal wurtzite structure of ZnO and correspond to the JCPDS data card (zinc oxide, 80–0074). In addition, the preferential

Table 1
The values of lattice parameters (a, c, and c/a), cell volume (V), profile value (Rp), weighted profile value (Rwp), the goodness of fit value ($\chi 2$), the crystallite size (L), dislocation density (δ), the residual stress (σ) and Zn–O bond length ($r_{Zn\text{-}O}$) determined from XRD measurements.

Samples	a (Å)	c (Å)	c/a	V(Å^3)	Rp (%)	Rwp (%)	$\chi 2$	L (Å)	δ (10^{-5} Å^{-2})	σ(GPa)	$r_{Zn\text{-}O}$ (Å)
ZnO	3.249	5.208	1.603	47.61	5.92	7.28	1.61	222.90	2.01	−0.18	1.977
Al–ZnO	3.255	5.210	1.601	47.79	4.98	6.50	1.96	150.46	4.42	−0.27	1.980
Ga-ZnO	3.259	5.222	1.602	48.05	5.01	6.37	1.78	164.48	3.70	−0.81	1.983
In–ZnO	3.261	5.219	1.600	48.06	4.64	5.91	1.83	228.34	1.92	−0.67	1.984

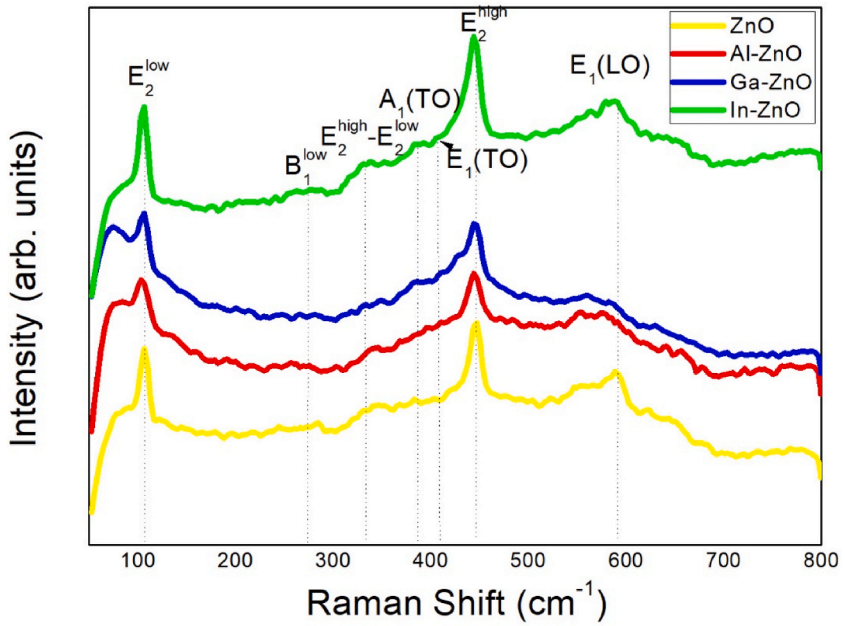

Fig. 2. Raman spectra of undoped and doped ZnO thin films.

orientation of the films is along the (002) and they have polycrystalline nature. As seen from the XRD patterns, the hexagonal wurtzite structure of ZnO remains unaltered with the addition of In, Al, and Ga atoms. The peak intensity of the XRD pattern corresponding to the (002) plane is observed to increase with In doping whereas decreases with Al and Ga doping atoms. This can be explained by the stress caused by the size remarkable difference between doping atoms involved in the film and Zn+2. Since atomic radii of Zn2+ and In3+ are close to each other, the stress in In-doped ZnO film is smaller [21]. Hence, the contribution of In+3 reduces the effect of ZnO crystallinity [22]. Similar behavior is also seen in In-doped ZnO films produced using the chemical bath storage method by Tyona et al. and using the sol-gel spin coating method by Bouainea et al. [19, 23]. Furthermore, the lattice parameters (a, c) and cell volume of the films are computed by the Rietveld method using a hexagonal structure with the space group P63mc and given Table 1. The crystallite size (L) is simply determined by Debye–Scherrer's formula:

$$L = \frac{0.9\lambda}{\beta cos\theta} \tag{1}$$

where λ, β, 2θ, and are the X-rays wavelength, the full width at half the maximum of the diffraction peak and the Bragg angle, respectively. The obtained L values are listed in Table 1.

As seen from Table 1, the lattice constants and cell volume of doped films are larger compared to undoped films. Although doping with different atoms increases the lattice parameters, the change in the c/a ratio indicating deviation from the wurtzite structure is small. The electronegativity of dopant atoms and Zn are not very different from each other and this is the reason why the change is small. As observed in Table 1, the crystallite size decreases in Al and Ga doped films, while it increases in In doped film. The number of defects in the films is described by dislocation density ($\delta = 1/L^2$). As seen in Table 1, the value of dislocation density decreases in In-doped film. So, this shows that the amount of defect decreases in In-doped films. Furthermore, the residual stress (σ) of doped ZnO films are determined by the following equation [24,25];

$$\sigma = -233\frac{\left(c_{film} - c_{bulk}\right)}{c_{bulk}}\ GPa \tag{2}$$

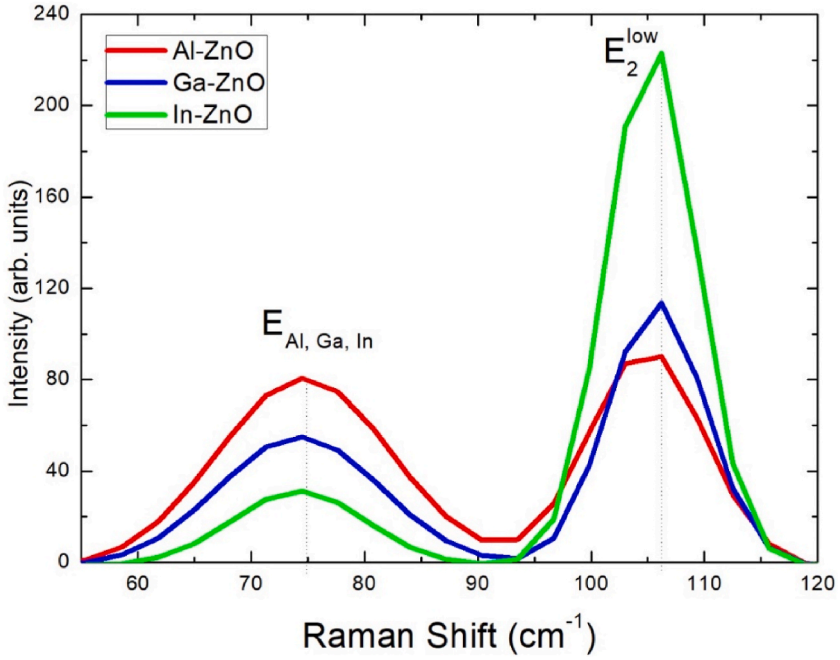

Fig. 3. Demonstration of Baseline and Gauss fitting for $E_{Al,\ Ga,\ In}$ and E_2^{low} peaks.

where c_{film} is the lattice constant of undoped and doped ZnO films and c_{bulk} (5.204 Å) is the stress-free constant of ZnO. The residual stress values of undoped and doped ZnO films are given in Table 1. The negative sign of stress (σ) reveals that the thin films are within compressive stress. For this reason, in our doped samples, the compressive stress is obtained in the direction c-axis. The quantity of stress relies on the nature of the contribution atom [26,27]. The Zn–O bond length, which is the measure of the distance between two neighboring Zn and O atoms at the lattice point, is calculated by the following equations and is given in Table 1.

$$r_{Zn-O} = \sqrt{\left[\frac{a^2}{3} + \left(\frac{1}{2} - u\right)^2 c^2\right]} \tag{3}$$

where u is the positional parameter related to the ratio of the lattice parameters, as given below

$$u = \frac{a^2}{3c^2} + 0,25 \tag{4}$$

The obtained values of $r_{Zn\text{-}O}$ deviate from the Zn–O bond length of 1.977 Å due to the lattice distortion caused by the doping atoms [28,29]. The results also confirm that no other impurity phases such as Ga–O (1.92 Å), Al–O (2.7 Å), and In–O (2.1 Å) are found in any of the produced samples [30].

3.2. Vibrational properties

Raman spectra demonstrated in Fig. 2 have prominent peaks at about 104 and 445 cm^{-1} and these peaks correspond to E_2^{low} and E_2^{high} modes of ZnO, respectively. E_2^{low} phonon branch is predominantly related to the motion of the Zn sub-lattice, while E_2^{high} mode is mostly formed by the vibration of oxygen atoms. The sharp E_2^{high} mode indicates good crystallinity of wurtzite ZnO. As seen in Fig. 2, the intensity of E_2^{high} mode increases in In-doped ZnO according to Al and Ga-doped ZnO films. According to XRD measurements, depending on the decrease in dislocation density of In-doped ZnO film, the number of defects decreases, and the crystallinity of film increases. As consistent with XRD results, Raman measurements show that the crystallinity of In-doped ZnO improves. Furthermore, the frequency of E_2^{high} virtually keeps unchanged by the doping. E_2^{high} mode which is resided at about 445 cm^{-1} in undoped, Al, and Ga-doped ZnO demonstrates a small change to 444 cm^{-1} in In-doped ZnO films. Since the E_2^{high} is strongly associated to the motion of O atoms, the frequency of this mode stays unaltered by the presence of Al, Ga, or In dopant atoms. Moreover, in the wurtzite crystal structure, the phonon mode of E_2^{high} is affected by the residual stress [31,32]. The residual stress (σ) is calculated using the following equation;

$$\sigma = \frac{\Delta\omega\ (cm^{-1})}{4.4}\ (GPa) \tag{5}$$

where $\Delta\omega$ is the variation of E_2^{high} mode frequency between doped ZnO and the stress-free bulk ZnO. The residual stress values are

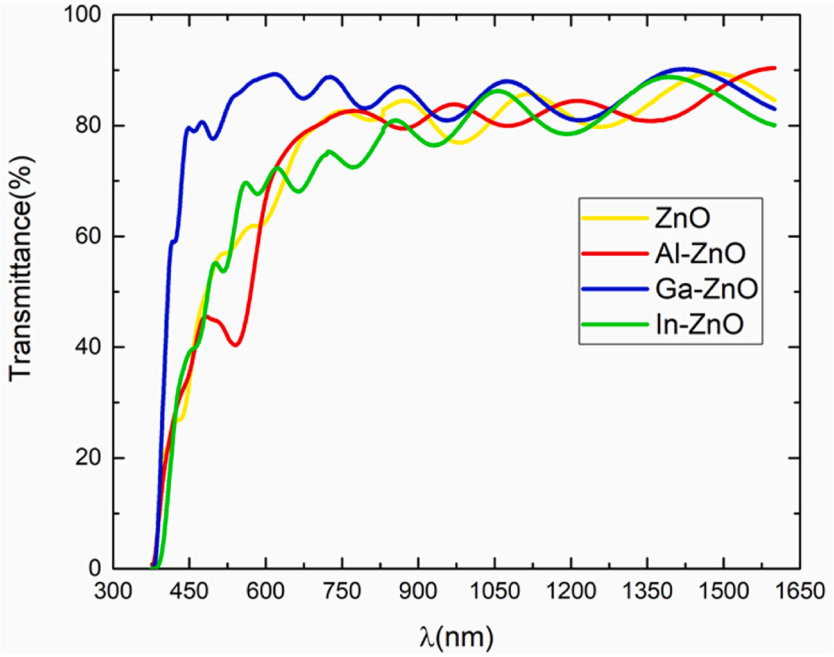

Fig. 4. Transmittance spectra of undoped and doped ZnO thin films.

determined as −1.93, −1.90, −1.89, and −1.64 GPa in the undoped and Al, Ga, and In-doped ZnO, respectively. Here, the frequency of stress-free bulk ZnO is considered as 437 cm^{-1}. It is well known that negative residual stress indicates compressive stress. According to these results, the residual stress value of In-doped ZnO decreases as consistent with XRD measurements.

As seen in Fig. 2, there are two peaks at near 576 and 588 cm^{-1} in Al-doped ZnO thin film. These peaks are associated with A_1(LO) and E_1(LO) phonon branches of ZnO, respectively [33]. In Ga and In-doped films, while the frequency of E_1(LO) mode remains unaltered at 588 cm^{-1}, the A_1(LO) mode approaches the E_1(LO) mode and appears as a single LO mode. The modes of A_1 and E_1 predominantly stem from the motion of oxygen atoms [34]. Since the bonds of Zn–O have ionic character, A_1 and E_1 branches are separated as longitudinal and transverse optical (LO and TO, respectively) phonons [35,36]. As observed in Fig. 2, while the A_1(TO) mode which is found at 384 cm^{-1} is vague in Al-doped ZnO, it has become more apparent in Ga and In-doped ZnO.

In addition to the main modes of ZnO, the anomalous vibrational modes are observed at 275 and 342 cm^{-1}. These modes correspond to B_1^{low} and multiphonon mode of E_2^{high}-E_2^{low}, respectively [37,38]. In Fig. 2, it is seen that the frequency of B_1^{low} mode stays unchanged in Ga and In-doped films. Moreover, as the ionic radius of the dopant atom increases, the E_2^{high}-E_2^{low} mode shifts to 340 and 335 cm^{-1} in Ga and In-doped films, respectively.

Furthermore, when compared with bare ZnO, an extra peak which is located at around 75 cm^{-1} is observed in low-frequency values of Al, Ga, and In-doped ZnO. In our previous work, we have shown with Density Functional Theory (DFT) and experimental results that the peak we observed at low frequency (about 75 cm^{-1}) forms by the dopant atom Ga [17]. The frequency of this peak is obtained as 74.69, 74.27, and 74.17 for Al, Ga and In doped films, respectively. So, a little phonon softening appears at this low-frequency peak as the radius and weight of the dopant atom increase. To examine the modes of low frequency, Baseline and Gauss fitting are applied to the low-frequency region (Fig. 3). As seen in Fig. 3, the intensity of E_2^{low} mode increases as the ionic radius of the dopant atom increases. The frequency of E_2^{low} mode is obtained as 104.9, 105.8, and 105.4 for Al, Ga, and In-doped ZnO films. Since the E_2^{low} peak is concerned with the motion of Zn atoms, the substitution of Al, Ga, and In by Zn affects the vibrational frequencies of the doped ZnO films. In Fig. 3, it is seen that there is an important correlation between the ionic radius of dopant atoms and the variations in the intensity ratio of the low-frequency peaks (E_2^{low} and $E_{dop.atom}$). The intensity ratio, I($E_{dop.atom}$)/I(E_2^{low}), was calculated as 0.87, 0.49, and 0.14 for Al, Ga, and In-doped ZnO films, respectively. It is seen that the intensity ratio, I($E_{dop.atom}$)/I(E_2^{low}), decreases as the ionic radius of dopant atoms increases.

3.3. Optical properties

The obtained transmittance spectra to investigate the optical properties of undoped and doped ZnO films are given in Fig. 4. It is seen that the films exhibit high transmittance and Ga doped ZnO film has 85% optical transmittance in the visible region and its transmittance in this region is higher than other films. The interference fringes are seen in the transmittance spectra because of the variation between glass substrate (s) and reactive index (n) of the film. The refractive indices of the films are obtained by applying Swanepoel's envelope method to these interference fringes [39]. The refractive index of the films is determined by the following equations;

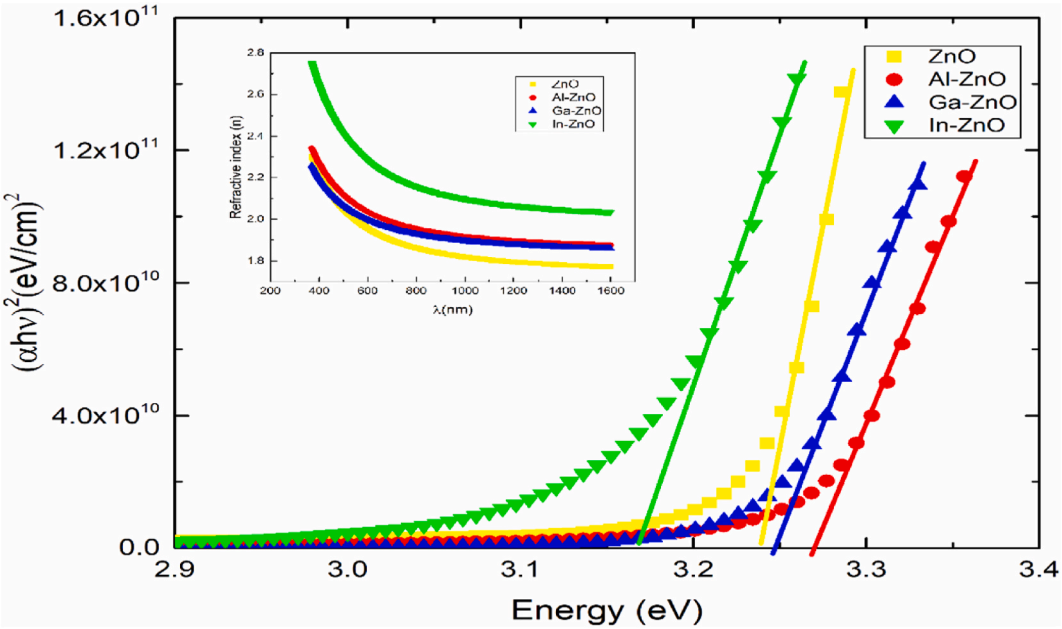

Fig. 5. $(\alpha h\nu)^2$ vs. $h\nu$ plots of the films. Inset: The variation of refractive index n with wavelength λ.

Table 2
The thickness (d), optical band gap (E_g), Urbach energy (E_u), and refractive index (n) values of the films were calculated from UV–Vis transmittance spectra.

Samples	d(nm)	E_g(eV)	E_u(meV)	n((λ = 550 nm)
ZnO	952	3.23	108.0	2.46
Al–ZnO	1154	3.27	141.4	2.07
Ga-ZnO	1089	3.25	85.2	1.99
In–ZnO	1046	3.17	145.2	2.34

$$n = \left[N + \left(N^2 - s^2\right)^{½}\right]^{½} \tag{7}$$

$$N = 2s\frac{T_M - T_m}{T_M T_m} + \frac{s^2 + 1}{2} \tag{8}$$

where s, T_M, and T_m are the refractive index of the substrate, the transmittance maximum value, and the corresponding minimum transmittance value for any λ in the envelope, respectively. The dependence of the refractive index on the wavelength is obtained by fitting the refractive index values experimentally found in the middle and weak absorption region of the transmittance spectrum to the two-term Cauchy dispersion relation $n = A + B/\lambda^2$. The dependence of the refractive index n on wavelength for undoped and doped ZnO films is given in the inset of Fig. 5. The refractive index values at 550 nm are given in Table 2 and the obtained values are compatible with those given in the literature [40].

The absorption coefficient (α) of the films are found by the following equation;

$$\alpha = \frac{1}{d} ln\left(\frac{1}{T(\lambda)}\right) \tag{9}$$

where d is film thickness and T is transmittance. Also, the optical energy band gap of the films (E_g) is obtained utilizing Tauc equation [41], $\alpha = \frac{A}{h\nu}(h\nu - E_g)^n$, which gives the relationship between absorption coefficients (α) and photon energy ($h\nu$). In Tauc equation, A, E_g, and n are a constant, band gap, and 1/2 for direct (2 for indirect) allowed transitions, respectively. The plot of $(\alpha h\nu)2$ vs $h\nu$ based on the Tauc equation for direct optical transitions is demonstrated in Fig. 5. The values of the band gap obtained by extrapolating the linear portions are also given in Table 2.

Depending on the type of doping atom, the amount of doping, and the crystallite size, different mechanisms affect the optical energy band gap value of the samples. It was found that the band gap narrowing mechanism caused by the existence of localized defect states into the forbidden band in In-doped ZnO films is effective and is consistent with the results of other researchers [19,23,26,42].

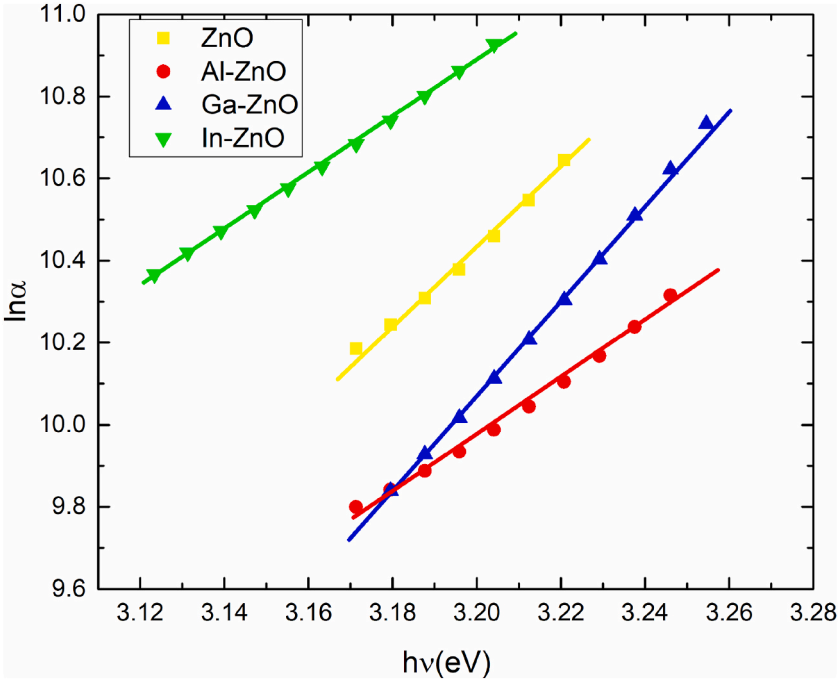

Fig. 6. lnα vs. hν plots of the films.

The Urbach energy value found for these films, which gives a measure of the disorder and width of the localized states entering the forbidden band, is greater than that of other doped films [43,44]. The optical energy band widening mechanism was found to be effective in Al and Ga doped ZnO samples with smaller crystallite sizes. Widening of the band gap values occurs due to the filling of the lowest state in the conduction band due to the doping effect known as the Burstein-Moss effect. The results are in agreement with previous studies [45,46].

The exponential relation between α and $h\nu$ near the band edge can be explained by the Urbach rule:

$$\alpha = \alpha_0 \exp\left(\frac{h\nu}{E_u}\right) \tag{10}$$

where α_0 , and E_u are a constant, and Urbach energy corresponds to the tail width below the band edge [47]. Rearranging Eq. (10) by taking the natural logarithm of both sides reveals a linear relationship between $ln\alpha$ and $h\nu$:

$$ln\alpha = ln\alpha_0 + \left(\frac{h\nu}{E_u}\right) \tag{11}$$

$ln\alpha$ vs $h\nu$ plots of undoped and doped ZnO films in the region close to the band edge are shown in Fig. 6. The tail widths (E_u) of thin films were found from the inverse slope of the linear regions of the graphs and are given in Table 2, the defect densities of each film can be compared with each other. The obtained results are in agreement with those presented in previous works [23,48,49].

4. Conclusions

In this study, the effect of doping with group III elements such as Al, Ga, and In on the characteristic properties of ZnO thin films formed by the sol-gel method is examined. The XRD spectra reveal that doped and undoped ZnO films have a wurtzite structure and the preferential crystallographic orientation of the films is c-axis oriented in the (002) plane. The peak intensity of the (002) plane decrease with Al and Ga doped films whereas increases with Indium doped film.

Due to the small difference in radius between İndium and Zinc, In doping does not reduce the crystallinity of the film. XRD measurements show that the crystallinity of the film increases due to the decrease in the dislocation density of the In-doped ZnO film. As consistent with XRD results, Raman measurements indicate that the crystallinity of In-doped ZnO improves. Raman and XRD measurements reveal that all of the films are under compressive stress, due to experimental conditions and the difference in radius between doping atoms and Zn. Furthermore, Raman spectra show that an additional peak which is located at around 75 cm^{-1} in low-frequency values of Al, Ga, and In-doped ZnO. Raman spectra also indicate that the intensity of E_2^{low} mode increases as the ionic radius of the dopant atom increases. Since the E_2^{low} mode is related to the motion of Zn atoms substitutional doping of the Zn atoms affects the vibrational frequencies of the Al, Ga, and In-doped films. It is also observed that the intensity ratio of $E_{dop.atom}$ and E_2^{low} which are

obtained at low frequency decreases as the ionic radius of dopant atoms increases. As seen from optical transmittance measurements while the refractive index value at 550 nm wavelength is 2.46 in bare ZnO, it shifts to 2.07, 1.99, and 2.34 in Al, Ga, and In doped films. The value of the optical band gap decreases from 3.23 to 3.17 eV in pure and indium doped ZnO, respectively, due to the expansion of crystallite size by indium doping. Similarly, the optical band gap increases to 3.27 and 3.25 eV, in Al and Ga doped films. The XRD, Raman, and optical results are in agreement with each other and our results manifest that structural, vibrational, and optical properties of ZnO film can be modified with the type of dopant atoms.

Author statement

Seyda Horzum: Writing – original draft, Visualization Emel Bulduk: Investigation Deniz Şener: Investigation Tülay Serin: Resources, Writing – original draft, Supervision

Declaration of competing interest

The authors declare that they have no known competing financial interests or personal relationships that could have appeared to influence the work reported in this paper.

Acknowledgments

This research did not receive any specific grant from funding agencies in the public, commercial, or not-for-profit sectors.

References

[1] H. Morkoç, Ü. Özgür, Zinc Oxide: Fundamentals, Materials and Device Technology, Willey-VCH publish, 2008.
[2] Ü. Özgür, D. Hofstetter, H. Morkoç, ZnO devices and applications: a review of current status and future prospect, Proc. IEEE 98 (2010) 1255–1268.
[3] V. Consonni, J. Briscoe, E. Kärber, X. Li, T. Cossuet, ZnO nanowires for solar cells: a comprehensive review, Nanotechnology 30 (2019) 362001.
[4] W. Dewald, V. Sittinger, W. Werner, C. Jacobs, B. Szyszka, Optimization of process parameters for sputtering of ceramic ZnO: Al_2O_3 targets for a-Si:H/μc-Si:H solar cells, Thin Solid Films 518 (2009) 1085–1090.
[5] S. Pati, P. Banerji, S.B. Majumder, Properties of indium doped nanocrystalline ZnO thin films and their enhanced gas sensing performance, RSC Adv. 5 (2015) 61230–61238.
[6] W.Z. Xu, Z.Z. Ye, Y.J. Zeng, L.P. Zhu, B.H. Zhao, L. Jiang, J.G. Lu, H.P. He, S.B. Zhang, ZnO light-emitting diode grown by plasma-assisted metal organic chemical vapor deposition, Appl. Phys. Lett. 88 (2006) 173506.
[7] L. Petti, N. Münzenrieder, C. Vogt, H. Faber, L. Büthe, G. Cantarella, F. Bottacchi, T.D. Anthopoulos, G. Tröster, Metal oxide semiconductor thin-film transistors for flexible electronics, Appl. Phys. Rev. 3 (2016), 021303.
[8] R.L. Hoffman, B.J. Norris, J.F. Wager, ZnO-based transparent thin-film transistors, Appl. Phys. Lett. 82 (2003) 733.
[9] M. Li, X. Qian, A.-D. Li, Y.-Q. Cao, H.-F. Zhai, D. Wu, A comparative study of growth and properties of atomic layer deposited transparent conductive oxide of Al doped ZnO films from different Al precursors, Thin Solid Films 646 (2018) 126–131.
[10] H.K. Park, J. Heo, Improved efficiency of aluminum doping in ZnO thin films grown by atomic layer deposition, Appl. Surf. Sci. 309 (2014) 133–137.
[11] A. Mitra, R.K. Thareja, V. Ganesan, A. Gupta, P.K. Sahoo, V.N. Kulkarni, Synthesis and characterization of ZnO thin films for UV laser, Appl. Surf. Sci. 174 (2001) 232–239.
[12] Q.A. Xu, J.W. Zhang, K.R. Ju, X.D. Yang, X. Hou, ZnO thin film photoconductive ultraviolet detector with fast photoresponse, J. Cryst. Growth 289 (2006) 44–47.
[13] A. Costas, C. Florica, N. Preda, N. Apostol, A. Kuncser, A. Nitescu, I. Enculescu, Radial heterojunction based on single ZnO-CuxO core-shell nanowire for photodetector applications, Sci. Rep. 9 (2019) 5553.
[14] P.K. Nayak, J. Jang, C. Lee, Y. Hong, Effects of Li doping on the performance and environmental stability of solution processed ZnO thin film transistors, Appl. Phys. Lett. 95 (2009) 193503.
[15] B.D. Ahn, H.S. Kang, J.H. Kim, G.H. Kim, H.W. Chang, S.Y. Lee, Synthesis and analysis of Ag-doped ZnO, J. Appl. Phys. 100 (2006), 093701.
[16] S. Horzum, E. Torun, T. Serin, F.M. Peeters, Structural, electronic and optical properties of Cu-doped ZnO: experimental and theoretical investigation, Philos. Mag. A 96 (2016) 1743–1756.
[17] S. Horzum, F. Iyikanat, R.T. Senger, C. Çelebi, M. Sbeta, A. Yildiz, T. Serin, J. Mol. Struct. 1180 (2019) 505–511.
[18] V. Russo, M. Ghidelli, P. Gondoni, C.S. Casari, A. Li Bassi, Multi-wavelength Raman scattering of nanostructured Al-doped zinc oxide, J. Appl. Phys. 115 (2014), 073508.
[19] M.D. Tyona, S.B. Jambure, R.U. Osuji, M. Maaza, C.D. Lokhande, F.I. Ezema, The effect of indium doping on photovoltaic properties of chemically synthesized zinc oxide thin-film electrodes, J. Solid State Electrochem. 24 (2020) 313–320.
[20] S. Zhuiykov, Nanostructured Semiconductor Oxides for the Next Generation of Electronics and Functional Devices: Properties and Applications, Woodhead Publishing Limited, 2014.
[21] P. Li-Ping, H. A-Ling, F. Liang, Y. Xiao-Fei, Structure and properties of indium-doped ZnO films prepared by RF magnetron sputtering under different pressures, Rare Met. (2015) 1–5.
[22] S. Girjesh, S.B. Shrivastava, J. Deepti, P. Swati, T. Shripathi, V. Ganesan, Effect of indium doping on zinc oxide films prepared by chemical spray pyrolysis technique, Bull. Mater. Sci. 33 (2010) 581–587.
[23] S. Bouainea, A. Bourebiaa, H. Guendouza, Z. Riane, Synthesis and characterization of in doped ZnO thin film as efficient transparent conducting oxide candidate, Optik 166 (2018) 317–322.
[24] Y.G. Wang, S.P. Lau, H.W. Lee, S.F. Yu, B.K. Tay, X.H. Zhang, K.Y. Tse, H.H. Hng, Comprehensive study of ZnO films prepared by filtered cathodic vacuum arc at room Temperature, J. Appl. Phys. 94 (2003) 1597–1604.
[25] O. Lupan, L. Chow, S. Shishiyanu, E. Monaico, T. Shishiyanu, V. Şontea, B. Roldan Cuenya, A. Naitabdi, S. Park, A. Schulte, Nanostructured zinc oxide films synthesized by successive chemical solution deposition for gas sensor applications, Mater. Res. Bull. 44 (2009) 63–69.
[26] C. Lung, M. Toma, M. Pop, D. Marconi, A. Pop, Characterization of the structural and optical properties of ZnO thin films doped with Ga, Al and (Al+Ga), J. Alloys Compd. 25 (2017) 1238–1243.
[27] B. Sahoo, D. Behera, S. KPradhan, D.K. Mishra, S.K. Sahoo, R.R. Nayak, K.P.C. Sekhar, Analysis of structural, optical and electrical properties of nano-particulate indium doped zinc oxide thin films, Mater. Res. Express 6 (2019) 1150a6.
[28] E.T. Seid, F.B. Dejene, Controlled synthesis of In-doped ZnO: the effect of indium doping concentration, J. Mater. Sci. Mater. Electron. 30 (2019) 11833–11842.

[29] H. Ennaceri, M. Boujnah, D. Erfurt, J. Rappich, X. Lifei, A. Khaldoun, A. Benyoussef, A. Ennaoui, A. Taleb, Influence of stress on the photocatalytic properties of sprayed ZnO thin films, Sol. Energy Mater. Sol. Cell. 201 (2019) 110058.
[30] S.J. Young, Y.H. Liu, M.D.N.I. Shiblee, K. Ahmed, L.T. Lai, L. Nagahara, T. Thundat, T. Yoshida, S. Arya, H. Furukawa, A. Khosla, Flexible ultraviolet photodetectors based on one-dimensional gallium-doped zinc oxide nanostructures, ACS Appl. Electron. Mater. 2 (2020) 3522–3529.
[31] C. Cong, H.Y. Hei, P.F. Zhang, W.Q. Peng, J.J. Wu, X.L. Liu, C.M. Jiao, W.G. Hu, Q.S. Zhu, Z.G. Wang, One-step growth of ZnO from film to vertically well-aligned nanorods and the morphology-dependent Raman scattering, Appl. Phys. Lett. 87 (2005) 231903.
[32] M.S. Kim, S. Kim, J.-Y. Leem, Laser-assisted sol-gel growth and characteristics of ZnO thin films, Appl. Phys. Lett. 100 (2012) 252108.
[33] F. Rubio-Marcos, C.V. Manzano, J.J. Reinosa, I. Lorite, J.J. Romero, J.F. Fernández, M.S. Martín-González, Modification of optical properties in ZnO particles by surface deposition and anchoring of NiO nanoparticles, J. Alloys Compd. 509 (2011) 2891–2896.
[34] V. Russo, M. Ghidelli, P. Gondoni, C.S. Casari, A. Li Bassi, Multi-wavelength Raman scattering of nanostructured Al-doped zinc oxide, J. Appl. Phys. 115 (2014), 073508.
[35] Ü. Özgür, Y.I. Alivov, C. Liu, A. Teke, M.A. Reshchikov, S. Doğan, V. Avrutin, S.-J. Cho, H. Morkoç, A comprehensive review of ZnO materials and devices, J. Appl. Phys. 98 (2005), 041301.
[36] A. Sahai, Y. Kumar, V. Agarwal, S.F. Olive-Méndez, N. Goswami, Doping concentration driven morphological evolution of Fe doped ZnO nanostructures, J. Appl. Phys. 116 (2014) 164315.
[37] A. Kaschner, U. Haboeck, M. Strassburg, M. Strassburg, G. Kaczmarczyk, A. Hoffmann, C. Thomsen, A. Zeuner, H.R. Alves, D.M. Hofmann, B.K. Meyer, Nitrogen-related local vibrational modes in ZnO:N, Appl. Phys. Lett. 80 (2002) 1909.
[38] A. Souissi, A. Boukhachem, Y. BenTaher, A. Ayadi, A. Mefteh, M. Ouesleti, S. Guermazi, M. Amlouk, Structural and vibrational studies of Mo and In-doped ZnO sprayed thin films, Optik 125 (2014) 3344–3349.
[39] R. Swanepoel, Determination of the thickness and optical constants of amorphous silicon, J. Phys. E Sci. Instrum. 16 (1984) 1214–1222.
[40] A. Kaphle, P. Hari1, Variation of index of refraction in cobalt doped ZnO nanostructures, J. Appl. Phys. 122 (2017) 165304.
[41] J. Tauc, Amorphous and Liquid Semiconductor, Plenum Press, London, New York, 1974.
[42] H.V. Thang, G. Pacchioni, Electronic structure of Al, Ga, in and Cu doped ZnO/Cu(111) bilayer films, Phys. Chem. Chem. Phys. 21 (2019) 369–377.
[43] J.P. McKelvey, Solid State and Semiconductor Physics, Robert E. Krieger Publishing Company Malabar, 1966.
[44] A. Hafdallah, F. Yanineb, M.S. Aida, N. Attaf, In doped ZnO thin films, J. Alloys Compd. 509 (2011) 7267–7270.
[45] L.C.-K. Liau, J.-S. Huang, Effect of indium- and gallium-doped ZnO fabricated through sol-gel processing on energy level variations, Mater. Res. Bull. 97 (2018) 6–12.
[46] C. Cong, H.Y. Hei, P.F. Zhang, W.Q. Peng, J.J. Wu, X.L. Liu, C.M. Jiao, W.G. Hu, Q.S. Zhu, Z.G. Wang, One-step growth of ZnO from film to vertically well-aligned nanorods and the morphology-dependent Raman scattering, Appl. Phys. Lett. 87 (2005) 231903.
[47] F. Urbach, The long-wavelength edge of photographic sensitivity and of the electronic absorption of solids, Phys. Rev. 92 (1953) 1324.
[48] T. Jannanea, M. Manoua, A. Liba, N. Fazouan, A. El Hichou, A. Almaggoussi, A. Outzourhit, M. Chaik, Sol-gel Aluminum-doped ZnO thin films: synthesis and characterization, J. Mater. Environ. Sci. 8 (1) (2017) 160–168.
[49] M. Hjiri, M.S. Aida, O.M. Lemine, L.E. Mir, Study of defects in Li-doped ZnO thin films, Mater. Sci. Semicond. Process. 89 (2019) 149–153.